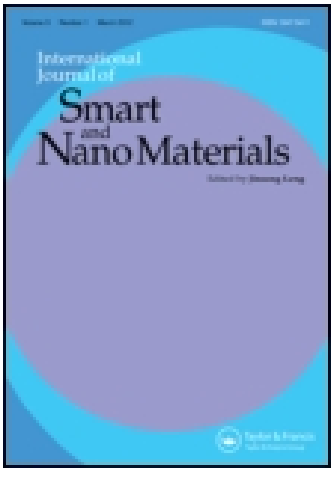

International Journal of Smart and Nano Materials

Publication details, including instructions for authors and subscription information:
http://www.tandfonline.com/loi/tsnm20

Long-range attractive forces extending from alumina nanofiber surface

Leonid A. Kaledin[a], Fred Tepper[a] & Tatiana G. Kaledin[a]

[a] Argonide Corporation, 291 Power Court, Sanford, FL 32771, USA

Published online: 25 Jul 2014.

To cite this article: Leonid A. Kaledin, Fred Tepper & Tatiana G. Kaledin (2014) Long-range attractive forces extending from alumina nanofiber surface, International Journal of Smart and Nano Materials, 5:3, 133-151, DOI: 10.1080/19475411.2014.919970

To link to this article: http://dx.doi.org/10.1080/19475411.2014.919970

International Journal of Smart and Nano Materials, 2014
Vol. 5, No. 3, 133–151, http://dx.doi.org/10.1080/19475411.2014.919970

Long-range attractive forces extending from alumina nanofiber surface

Leonid A. Kaledin*, Fred Tepper and Tatiana G. Kaledin

Argonide Corporation, 291 Power Court, Sanford, FL 32771, USA

(*Received 25 October 2013; final version received 28 April 2014*)

Aluminum oxide-hydroxide nanofibers, 2 nm in diameter and approximately 250 nm long, are electroadhesively grafted onto glass microfibers, therefore forming a macroscopic assembly of alumina nanofibers on the second solid in highly organized matter. The assembly can be viewed as a straight cylinder with rough surface and charge density of approximately 0.08 C/m^2. This creates a significant electric field with negligible screening ($ka \ll 1$) in the region close to the surface of the assemblies. This field attracts nano- and micron-size particles from as far as 0.3 mm in less than a few seconds, many orders of magnitude greater than the conventional Derjaguin–Landau–Verwey–Overbeek theory that predicts only nanometer-scale effects arising from the presence of the surface. The strong electric field on the surface is then able to retain particles such as micron-size powdered activated carbon as well as much smaller particles such as fumed silica nanoparticles of 10–15 nm in diameter, viruses, atomically thick sheets of graphene oxide, latex spheres, RNA, DNA, proteins, and dyes.

Keywords: alumina nanofibers; electric double layer; electrostatic adsorption

1. Introduction

Electrically driven motion of solid particles in liquid electrolytes has been studied for more than a century in the field of colloid science. Electrokinetic phenomena are associated with the electric double layer (EDL) on charged surfaces of particles immersed in electrolyte solutions. Gouy and Chapman developed a diffuse layer (DL) theory [1,2]. Stern extended that theory by proposing a model in which the interfacial layer is divided in two parts [3], which can be further divided by the inner Helmholtz plane and the outer Helmholtz plane [4]. It has been shown [5] that the Stern model is a good *effective* model away from the surface, but cannot be taken literally near the surface. Static double DL are electroneutral, meaning that the surface charge σ^0 is exactly compensated by the counter-charge. The latter consists of two parts, one in the stagnant layer, σ^i and one in the 'electrokinetically active' part, σ^{ek}. In most cases, σ^i closely coincides with the non-diffuse Stern layer, part of the double layer. The σ^{ek} can be determined from electrokinetics (e.g., from measuring zeta potential, ζ [4]) and σ^0 can be determined from titration of surface groups [6] and their difference can be used to obtain σ^i. Often σ^{ek} is much less than σ^0, e.g., in the case of SiO_2 [7].

In the case of a flat DL, there is only one parameter, the Debye length, $1/k$, while in the case of a spherical or cylindrical DL, there is an additional geometric parameter, the

*Corresponding author. Email: kaledin@argonide.com

radius of the particle, a. A vast majority of aqueous dispersions satisfy the $ka \gg 1$ condition (thin DL) where the DL depth is much thinner than the particle radius while the $ka \ll 1$ condition (thick DL) where the DL depth is much larger than the particle radius. Theoretical treatments have been suggested for the thin DL ($ka > 10$) and for the thick DL ($ka < 1$) that include DL overlap [8]. At high electrolyte ionic strengths (>1 M), the Debye length becomes comparable with the size of the ions, implying that the DL collapses onto the particle surface. However, there are indications that in some cases, the DL still exists even at ionic strengths greater than 1 M [8].

Colloid stability is often predicted by the Derjaguin–Landau–Verwey–Overbeek (DLVO) theory [9,10], which was developed for smooth, homogeneous particles with ideal geometries and with no DL overlap. The electrostatic repulsive part of the potential between surface and solution is thought to drop off as e^{-rk}, where r is the distance from the surface and k is the inverse of the Debye length of the solution [11]. For example, in a 100 mM/dm^3 electrolyte solution, the Debye length is 1 nm [12], and a 2×10^4-fold potential drop is expected at a very short distance (~10 nm) from the surface. Moreover, the majority of the colloids have irregular geometries with rough surface [13] and heterogeneous composition. Despite the success of DLVO theory, numerous investigators have modified the DLVO theory to include factors not accounted for in the DLVO model, e.g., when live biological cells suspended in concentrated solutions of inorganic electrolytes around some cells (leukocytes, especially tumor cells) form haloes, i.e., circular spaces free from background cells (erythrocytes, yeast cells, and colloidal particles of Indian ink). In the medium made up of erythrocytes, the haloes form in 5–10 min as a result of the background cells drawing apart from the central halo-forming cell at a distance of 10–100 μm and more [14]. In the medium made of the Indian ink particles, the haloes form in 2–4 s and attain a thickness of about 10–20 μm [14]. Rivera et al. observed field patterns characteristic of repulsion and attraction [15] as well as dipolar and quadripolar nature. Theoreticians such as Pohl, the inventor of dielectrophoresis [16], Derjaguin, the leading author of DLVO theory [9], and others have suggested three theoretical models, presumably to explain these experiments. Review articles by Dukhin et al. [17], Murtsovkin [18], and Bazant et al. [19] discussed in detail these unusual interaction mechanisms that are only specific for live biological cells.

Sogami suggested a different interpretation of colloidal forces [20]. The Sogami–Ise theory [21] claims that the attraction between colloidal particles comes from the influence of intervening ions. The Sogami potential contains both short-range repulsion and long-range attraction. This gives the attraction a longer reach than that in DLVO theory. The most conclusive findings were the observations of void structures of on the order of 25–50 μm in highly purified dispersion of latex particles [22–25] and long-range exclusion zones of latex microspheres on the order of 100 μm from the gel surface [26,27]. Recently, Sogami argued that the colloid dispersion is homogeneous with respect to variable T (Sogami–Ise theory [21]), and it is not with respect to volume, V (DLVO theory), which is not a suitable thermodynamic variable [28]. The screened Coulombic potential of pure repulsion obtained from the Helmholtz free energy in the DLVO theory was replaced by a new screened electric potential with a long-range attractive tail derived from the generalized Gibbs free energy, which is identified with the total sum of chemical potentials [28]. In this article, we report on long-range attractive forces extending from an alumina (aluminum oxide-hydroxide (AlOOH)) nanofiber surface.

2. Materials and methods

2.1. *Alumina nanofiber electropositive filter*

A novel water purification filter is in the process of development over the past 10 years [29]. The filter's active component is an alumina monohydrate nanofiber with an external surface area from 200 to 650 m^2/g [29]. It has been identified as crystalline pseudoboehmite (AlOOH) using X-ray diffraction [30]. Figure 1 shows transmission electron microscopy (TEM) and scanning electron microscopy (SEM) images of the alumina nanofibers bonded to a glass microfiber prepared as described in Example 4 in Ref. [29].

The isoelectric point (IEP or pI) of alumina raw fibers is approximately 11.1 [31]. Micron-size and nanosize particles were readily held by electrostatic forces while forming the nonwoven paper-like sheet [29]. For instance, a 30 × 30-cm^2 handsheet was prepared containing 28 weight percent (wt%) of fumed silica with average particle size of ~10 nm [30]. The fumed silica that is very difficult to filter from aqueous mixtures was rapidly clarified to form a clear suspension. The resulting handsheet had a low differential pressure drop of 10 kPa at flow velocity of 0.7 mm/s that is not characteristic of filtered colloidal silica. When examined under the electron microscope, we noted that the silica nanoparticles were clinging to the alumina nanofibers (Figure 2(a)). Handsheets (30 × 30 cm^2) were also formed containing atomically thick sheets of graphene oxide (up to 40 wt%), 50 nm titanium dioxide (12 wt%), and RNA (5 wt%). The result was a nanoengineered media that could retain and utilize the function of virtually any submicron or nanosize particle [30]. A practical application was focused on integrating powdered activated carbon (PAC) with average particle size of ~8 μm into the nonwoven structure (Figure 2(b)). Activated carbon has a large amount of its surface area within micro-pores of about 0.2–2 nm in diameter [32]. At the same time, the dimensions of the pore have a significant impact upon diffusion rates of adsorbed molecules through the granule. Generally, diffusion rates are determined by the mean free path length of the molecules being adsorbed. The smaller the pores the longer is the mean free path length and the slower the diffusion rates [33]. By substantially reducing the particle's size, one could reduce the length through the tortuous mesopore and micropore structures, thereby increasing the adsorption rate.

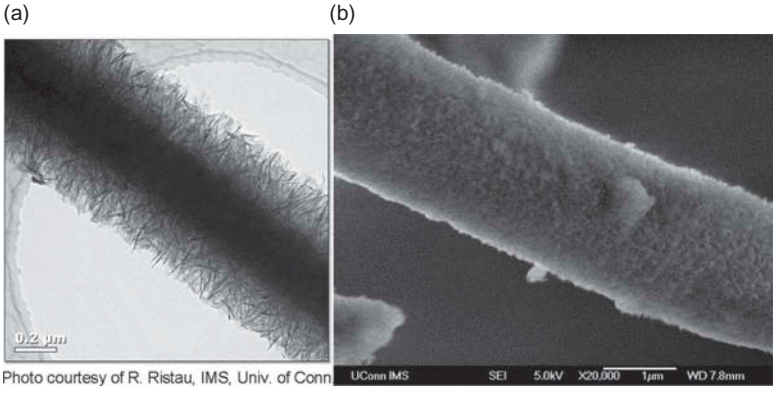

Figure 1. (a) TEM image of alumina nanofibers bonded to glass microfiber; (b) SEM image shows a carpet of alumina nanofibers completely covering the glass microshaft.

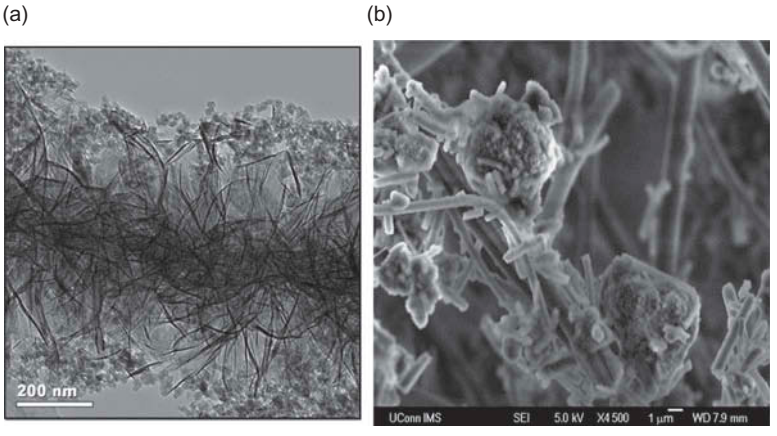

Figure 2. (a) Silica nanoparticles deposited on alumina nanofiber/lyocell microfiber; (b) SEM image of PAC in alumina nanofiber/glass microfiber.

2.2. Mulch preparation

For the purpose of this study, the alumina nanofiber content was optimized at 40 wt% (R = 0.4) to 60 wt% of glass microfibers ($1 - R$) so that the alumina nanofibers cover densely the available surface on the 0.6-μm glass microfiber scaffolding. No other fibers or binders were added to the mulch. Since the crystalline structure of nanofibers was identified as pseudoboehmite (AlOOH) [30], the 40 wt% of the alumina nanofibers was obtained by mixing the aluminum and glass microfibers in deionized reverse osmosis (DI RO) water in a proportion of 27 g of Al powders to 60 g of glass microfibers to obtain 40 g of AlOOH nanofibers deposited onto 60 g of glass microfibers. The solid load in the prepared mulch was M/V = 6 g/L where M is the mass of the assemblies dispersed in water. The total surface area of alumina nanofibers, S_{AlOOH}, can be estimated as:

$$S_{AlOOH} = N_{AlOOH}\pi d_{AlOOH} l_{AlOOH} \cong \frac{4RM}{d_{AlOOH}\rho_{AlOOH}} \tag{1}$$

where

$$N_{AlOOH} \cong \frac{RD_{glass}^2 L_{glass}\rho_{glass}}{(1-R)d_{AlOOH}^2 l_{AlOOH}\rho_{AlOOH}} = \frac{4RM}{\pi d_{AlOOH}^2 l_{AlOOH}\rho_{AlOOH}} \tag{2}$$

D_{glass}, L_{glass}, and ρ_{glass} are the diameter, length, and density of the glass microfiber, respectively, and d_{AlOOH}, l_{AlOOH}, and ρ_{AlOOH} are the diameter, length, and density of the nanofiber.

Unit cell parameters for crystalline boehmite are [34] as follows: a = 0.2768 nm, b = 1.2227 nm, and c = 0.3700 nm. Assuming that alumina nanofibers grow by the longest side b of the cell oriented along the length of nanofiber, an estimation shows that 25 cells with a and c sides form a layer within a 2 nm diameter from which 13 cells (or ~50% of all cells) lie on the outside boundary layer. The average length of alumina nanofiber is 250 nm, therefore 20 layers with b side oriented along the length of the fiber.

The positive charge of the Al^{3+} ions situated close to the surface of each nanofiber is $3 \cdot e \cdot 13 \cdot 20 = 780 \cdot e$, where e is an elementary charge with total charge, Q_{AlOOH}, on the assembly and on the top layer

$$Q_{AlOOH} = 780e \times N_{AlOOH} = M \times 1.6 \cdot 10^{20} \mathrm{e/g} = \mathrm{M} \times 25.4\ \mathrm{C/g} \tag{3}$$

$$Q_{AlOOH}^{top\ layer} = 75e \times N_{AlOOH} = 2.4 \times M\ \mathrm{C/g} \tag{4}$$

and with the linear λ^0 and surface σ^0 charge density values

$$\lambda^0 = \frac{Q_{AlOOH}^{top\ layer}}{L_{glass}} = \frac{2.4\pi D_{glass}^2 \rho_{glass}}{4(1-R)} = 2.8\mu\mathrm{C/m} \tag{5}$$

$$\sigma^0 = Q_{AlOOH}/S_{AlOOH} \approx 0.08\,\mathrm{C/m^2} \tag{6}$$

where ρ_{glass} = 2.5 g/cm^3. The estimated σ^0 value is in good agreement with an experimental value of ~2–10 μC/cm^2 of boehmite nanoparticles with a surface area of 124 m^2/g in a solution of 10^{-2} M NaCl at pH in the range from 6 to 8 [35].

The length of dried assemblies was determined by plotting a discrete density distribution histogram of assembly lengths with the use of an optical microscope. The median length $l_{assembly}$ was determined at the 50% point of the cumulative curve, and the width of the distribution was determined as ratios of the length at 16% and 84% on the cumulative curve [36]. L_{glass} is the total lengths of all microglass fibers, l_{glass}, linked together to form a straight cylinder, that is, $L_{glass} = \sum l_{glass}$. The median length $l_{assembly}$ of the assemblies ($l_{glass} = l_{assembly}$) for the above prepared mulch was found to be 168^{+192}_{-108} μm. Assuming that each of the NanoCeram® assemblies surrounded by a volume of water with a cross section of $A \times A$ and length l_{glass}, the resulting size of the cross section does not depend on the length of l_{glass}:

$$A = \sqrt{\frac{V}{L_{glass}}} = \sqrt{\frac{\pi \cdot V \cdot \rho_{glass}}{4(1-R) \cdot M}} D_{glass} \tag{7}$$

where A = 14 μm for M/V = 6-g/L loading. The mulch was divided into several parts, diluted with DI RO water at ratios of 1:20 and 1:250, and pH was adjusted with either HCl or NaOH by using Oakton pH2700 pH-meter. Table 1 presents the results.

2.3. *Latex beads*

Monodispersed polystyrene latex microspheres (beads) coated with sulfate groups with a mean diameter of 30 ± 5 nm were obtained from Duke Scientific Corporation. According to the manufacturer, the spheres have a net negative charge in aqueous solution. Particles were used as supplied by the manufacturer and resuspended in DI RO water whose conductivity is less than 0.1 μS/cm as measured by an Oakton ECTestr 11 conductivity meter. The charge is provided by a mixture of sulfate and hydroxyl groups on the latex surface with zeta potential of approximately −82 mV [37].

Table 1. Characteristics of alumina nanofiber mulches.

Solid load (g/L)	Dilution factor	pH	λ_m (mS/cm[a])	Ionic strength (Na^+ or Cl^-) (mM)	$1/k$ (nm)[b]	Average distance between two assemblies, $2A$ (μm)[c]	ka[d]
6	1:1	9	5.8	50	1.4	28	0.7
		7	5.8	50	1.4	28	0.7
		5	6.3	50	1.4	28	0.7
		3	12.1	100	1.0	28	1.0
0.3	1:20	9	0.94	2.5	6.3	125	0.16
		7	0.46	2.5	6.3	125	0.16
		5	0.50	2.5	6.3	125	0.16
		3	1.3	5	4.4	125	0.23
0.024	1:250	9	0.238	0.2	22	443	0.045
		7	0.118	0.2	22	443	0.045
		5	0.056	0.2	22	443	0.045

Note: [a]Conductivity of the medium; [b]Debye length. For 1:1 electrolyte, the double-layer thickness, $1/k$, is estimated according to Ref. [12] (see text for details); [c]Equation (7); [d]a is the radius of the alumina nanofiber (~1 nm).

2.4. Virus and bacteria isoelectric points

The pH value at which the net surface charge switches its sign is referred to as the isoelectric point and is a characteristic parameter of a virus in equilibrium with its environmental water chemistry. The IEP value of MS2 bacteriophage in different environments based on averaging of 10 measurements shows a mean IEP value of 3.5 ± 0.6 and with the discrepancy in IEP (ΔIEP) of 1.8 from 2.2 to 4.0 [38]. Two recent studies by Duek et al. [39] and Chrysikopoulos et al. [40] determined the alteration of the IEP by a change in water chemistry (e.g., ionic strength or ionic composition) with IEP of the former case in the range from less than 2 at ionic strengths of 0.0 and 2.6 mM to IEP of 4.4 in the latter case that was measured in double distilled water. In the case when clean colloidal particles are suspended in absolute pure water, the point of zero charge (PZC), which is characteristic to the particle' surface, can be determined. The IEP and the PZC do not necessarily differ in the presence of monovalent ions; however, the PZC is very difficult to measure experimentally [38].

MS2 (ATCC 15,597-B1) and *fr* (ATCC 15,767-B1) bacteriophages are icosahedral in shape with a diameter of 26–27 [39] and 19 nm [41], respectively. The IEP of *fr* bacteriophage is 8.9–9.0 [41]. In this study, MS2 bacteriophage was chosen because it is often used as a surrogate for human enteric viruses and *fr* bacteriophage was chosen because it is electropositive in aqueous suspensions at pH in the range from 3 to 9.

The *Escherichia coli* bacterium is Gram-negative, rod-shaped, with a cell IEP of 3.5 and zeta potential of $\zeta \sim -35$ mV that is fairly insensitive to pH from pH 6 to pH 9 [42]. The zeta potential of MS2 ($\zeta_{MS2} \sim -(33–38)$ mV [40]) is similar to that of *E. coli*.

2.5. Bacteriophages and bacteria preparation

Stocks of MS2 and *fr* bacteriophages with concentrations of ~10^{10} particles/mL and ~10^8 particles/mL, respectively, were stored at 4°C and then diluted in DI RO water with conductivity less than 0.1 μS/cm.

Stocks of *E. coli* (ATCC 15,597), *Raoultella terrigena* (ATCC 33,257), and *Acholeplasma laidlawii* (ATCC 14,089) with concentrations of ~10^9 particles/mL were stored at 4°C and then diluted in DI RO water with conductivity less than 0.1 μS/cm.

3. Results and discussion

3.1. MS2 bacteriophage adsorption by alumina nanofiber assembly

Three milliliters of well mixed mulch was transferred into a 15-mL sterile centrifuge tube and 3 mL of MS2 suspension was added whose input concentration was ~1.0×10^9 PFU/mL with a conductivity of ~28 μS/cm. The contents were allowed to dwell either for 30 s for a 3-g/L loading or for 8 min for 0.15- and 0.012-g/L loadings. The tubes were then centrifuged for 5 min at 1300 *g*. The supernatant was serially diluted by a factor of 10 and analyzed as plaque forming units with the use of the double-layer method [43]. Briefly, dilutions of each sample were mixed with host cells, plated on nutrient agar, and incubated overnight. The resulting plaque counts were converted to PFU/mL. Table 2 shows the results that indicate that at 3-g/L loading, water becomes biologically safe with respect to virus reduction requirement of 4 logarithm ($\log_{10}$) reduction value (LRV) [44] after a contact time of 30 s and at 0.15-g/L loading after 8 min in a wide pH range from 5 to 9. It should be noted that the mean length of l_{glass} ~ 168 μm is smaller than the average distance between two neighboring fibers ($2A$) for solid loadings of 0.15 and 0.012 g/L.

3.2. Electric field extension

We define electric field extension from alumina nanofiber surface to be equal to a distance that a small particle travels from the farthest point P in the plane of the assembly with $x = 0$ at the center and $y = r_0$ to the surface of the assembly during a certain time interval. Assuming that the assemblies around a particle are arranged in a form of a $3D$ symmetry

Table 2. MS2 bacteriophage adsorption by alumina nanofiber assembly.

Solid load (g/L)	pH	λ_m (mS/cm)[a]	$1/k$ (nm)[b]	Average distance between two assemblies (μm)	Contact time (min)	MS2 adsorption (LRV)[c]	ka[d]
3	10.7	2.9	2.0	40	0.5	1.9 ± 1.0	6.5
	9	2.9	2.0	40	0.5	4.4 ± 0.7	6.5
	7	2.9	2.0	40	0.5	5.7 ± 1.0	6.5
	5	3.2	2.0	40	0.5	4.6 ± 0.8	6.5
	3	6.1	1.4	40	0.5	2.5 ± 1.2	9.3
0.15	10.7	0.48	8.9	177	8	0.13 ± 0.18	1.5
	9	0.48	8.9	177	8	4.0 ± 1.4	1.5
	7	0.24	8.9	177	8	7.6 ± 0.3	1.5
	5	0.26	8.9	177	8	5.2 ± 0.5	1.5
	3	0.67	6.3	177	8	1.7 ± 0.3	2.1
0.012	9	0.133	32	626	8	0.6 ± 0.3	0.4
	7	0.073	32	626	8	0.9 ± 0.2	0.4
	5	0.042	32	626	8	5.4 ± 0.6	0.4

Note: [a]Conductivity of the medium; [b]Debye length (see footnote 'b' in Table 1); [c]logarithm ($\log_{10}$) reduction value; [d]a is the radius of MS2 bacteriophage.

Table 3. Electric field extension[a] from alumina nanofiber surface (μm).

Solid load (g/L)	pH	Resistivity (Ω·m)	Ionic strength (Na^+ or Cl^-) (mM)	$1/k$ (nm)[b]	Average distance between two assemblies $2A$ (μm)[c]	MS2 removal (LRV)	Depth of electric field extension, r_0 (μm)[d]	ka[e]
0.15	9	21	1.25	8.9	177	4.0 ± 1.4	84	1.5
	7	42	1.25	8.9	177	7.6 ± 0.3	88	1.5
	5	38	1.25	8.9	177	5.2 ± 0.5	87	1.5
	3	15	2.5	6.3	177	2.5 ± 0.8	76	2.1
0.012	9	76	0.1	32	626	0.6 ± 0.3	116	0.4
	7	137	0.1	32	626	0.9 ± 0.2	156	0.4
	5	238	0.1	32	626	5.4 ± 0.6	308	0.4

Note: [a]Measured with the use of MS2 bacteriophage; [b]Debye length (see footnote 'b' in Table 1); [c]Equation (7); [d]Equation (8); [e]a is MS2 radius.

(e.g., a sphere with diameter of $2A$ or a cube with side of $2A$), the removal efficiency of the particle from the suspension could be used to estimate r_0:

$$r_0 = A\left(1 - \sqrt[3]{\frac{C_{final}}{C_{initial}}}\right) \tag{8}$$

where $C_{initial}$ and C_{final} are the initial and final concentrations of particles. We chose MS2 bacteriophage as a model particle to measure r_0 as a function pH because its electrophoretic mobility is fairly insensitive to pH in the range of $4.5 < pH < 9.0$ and because $\zeta_{MS2} \sim -(36–38)$ mV [39] that is fairly insensitive to pH from pH 7 to pH 9.5. Table 3 and Figure 3 present the results, which show that the farthest reach of electric field to attract and collect MS2 particles at 8-min contact time is 0.3 mm. Moreover, the depth of electric field extension can be approximated by a linear function of electrolyte resistivity with the extrapolated value in a high salinity water of about 50 μm, which explains the MS2 removal efficiency that is greater than 99.9997% at NaCl concentration of 200 g/L by two layers of alumina nanofiber–PAC media with average pore size of 2 μm and at flow velocity of 0.7 mm/s [45].

3.3. *Mechanism*

It is apparent that the assembly structure presented in this work possesses a combination of several unique features:

(1) The screening around the nanofibers becomes negligible ($ka \ll 1$) at electrolyte strengths less than ~10 mM ($ka \sim 0.3$).
(2) As a result, the entire volume of aqueous suspension becomes electropositively charged within the alumina nanofiber layer of 250 nm deep that appears as a fuzzy region on the glass microfiber core (Figure 1(a)).
(3) The entire electropositive volume within the fuzzy region together with the top ends of the nanofibers further repel the electronegative screening layer around the entire assembly especially at low ionic strengths.

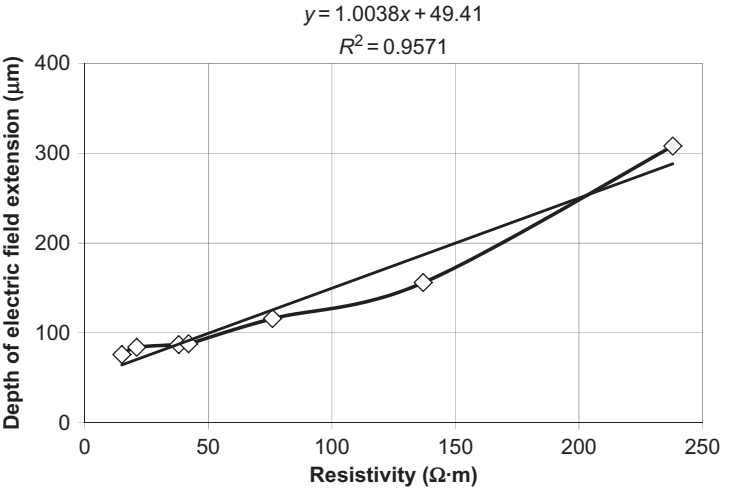

Figure 3. Extension of electric field from alumina nanofiber surface as a function of electrolyte resistivity.

(4) The resulting polarization field extends far beyond the DL. The *near field* has a range of O(1/k) and the *far field* of O(a) [46], where a is the radius of the assembly (~0.55 μm).
(5) As a result, the expressions for the potential ψ(r) and for the strength of electric field $\vec{E}(r)$ acquire the forms of a charged cylinder without countercharge in the range close to the assembly (*near field*) estimated at ~6–32 nm (see Table 3 for 0.15- and 0.012-g/L loadings), that is, the Coulomb case, and both functions decay as 1/r, where r is the distance from the assembly surface. This range is comparable with the radius of some bacteriophages (e.g., MS2 and *fr*).

If we place the cylinder on the x axis with the origin on the center, we can determine the electric field on a point P on the y axis at $y = r_0 > 0$; the magnitude dE of the electric field (at point P) caused by the charge d$Q = \lambda$dx on the x axis is given by [47]:

$$\mathrm{d}E = \frac{\mathrm{d}Q}{4\pi\varepsilon_0\varepsilon_m r^2} \tag{9}$$

where $r = r_0 \cdot \sec\theta$, θ is the angle at point P between r_0 and r, ε_0 is the dielectric permittivity of vacuum, $\varepsilon_0 = 8.8542 \times 10^{-12}$ C^2/J·m, and ε_m is a dielectric constant of dispersive medium with respect to vacuum. Integration from θ_1 to θ_2 where θ_1 is the angle at point P between r_0 and r_{left}, where r_{left} is the radius vector from point P to the left side of the assembly, and θ_2 is the angle at point P between r_0 and r_{right}, where r_{right} is the radius vector from point P to the right side of the assembly in the x–y coordinate plane gives:

$$E_x = -\frac{\lambda^0}{4\pi\varepsilon_0\varepsilon_m r_0}\int_{\theta_1}^{\theta_2} \sin\theta \mathrm{d}\theta \tag{10}$$

$$E_y = \frac{\lambda^0}{4\pi\varepsilon_0\varepsilon_m r_0}\int_{\theta_1}^{\theta_2}\cos\theta \mathrm{d}\theta \tag{11}$$

Thus, the electric field at point P is

$$\vec{E} = (E_x\vec{i} + E_y\vec{j}) \tag{12}$$

In the limiting cases:

(1) when a small particle ($a \ll$ L) is close to the assembly, integrating from $\theta_1 = -\pi/2(x \to -\infty)$ to $\theta_2 = \pi/2(x \to \infty)$ gives $E_x = 0$ and

$$E_y = \frac{\lambda^0}{2\pi\varepsilon_0\varepsilon_m r} \tag{13}$$

(2) when a small particle at point P ($x = 0$, $y = r_0$) is at one half of the distance between assemblies, $2A$, integrating from $\theta_1 = -\pi/4(x = -r_0)$ to $\theta_2 = \pi/4(x = r_0)$ gives $E_x = 0$ and

$$E_y = \frac{\lambda^0}{2\sqrt{2}\pi\varepsilon_0\varepsilon_m r_0} \tag{14}$$

It is important to note that a particle together with surrounding its 'screening DL' is electroneutral in a suspension, and in the case of nonlinear 'induced – charge' electrokinetic phenomena [16–19] such as dielectrophoresis and electrorotation, the part of the total force and torque applied to the screened particle influences both the EDL movement and the particle itself. Polarization effect induced on a screened particle by a static external field created by the nanoassembly in suspension can be described as [48]:

$$\overrightarrow{p}^{ind}_{screened} = \gamma^{ind}_{screened}\overrightarrow{E} \tag{15}$$

where $\overrightarrow{p}^{ind}_{screened} = \overrightarrow{p}^{ind}_{particle} + \overrightarrow{p}^{ind}_{EDL}$ and $\gamma^{ind}_{screened} = \gamma^{ind}_{particle} + \gamma^{ind}_{EDL}$ are induced dipole moment of the screened particle and its effective unitless polarizability, respectively. If the particle is charged, a significant increase in the equilibrium Debye atmosphere results in an increase of the force acting on it and may become comparable or higher than the force applied directly to the particle [48]. As a result, the effective polarizability of a screened particle at $ka \ll 1$ can greatly exceed (see Figure 5.7a in Ref. [48].) the maximum polarizability value $\gamma_{\max}(\varepsilon_m, a) = 4\pi\varepsilon_m\varepsilon_0 a^3$ of a sphere of radius a in a medium with permittivity ε_m. More detail estimation of polarizability value $\gamma_{\max}(\varepsilon_m, a)$ that includes surface and dispersive medium conductivities is given in Ref. [8] (see Equation (2.38)).

The total force acting on a polarized screened particle in a nonuniform electric field is given as [16]:

$$\overrightarrow{F}^{ind}_{screened} = \left(\overrightarrow{p}^{ind}_{screened}\cdot\nabla\right)\overrightarrow{E} = \gamma^{ind}_{screened}\left(\overrightarrow{E}\cdot\nabla\right)\overrightarrow{E} \tag{16}$$

The total torque of electric forces acting on a screened particle with induced dipole moment $\overrightarrow{p}^{ind}_{screened}$ is expressed as a cross product [48]:

$$\overrightarrow{M}^{ind}_{screened} = \overrightarrow{p}^{ind}_{screened} \times \overrightarrow{E} \tag{17}$$

The dielectric velocity $v^{de}_{screened}$ is calculated by equating the total force acting on a polarized screened particle and Stokes viscous force:

$$v^{de}_{screened} = \frac{4\pi e_m e_0 \left(\gamma^{ind}_{particle} + \gamma^{ind}_{EDL}\right)}{6\pi\mu a} \left(\overrightarrow{E}\cdot\nabla\right)\overrightarrow{E} \tag{18}$$

where μ is the viscosity of the dispersion medium and a is the particle's radius. Substituting Equations (13) and (16) in Equation (18), we obtain the following:

$$v^{de}_{screened} = \frac{\left(\gamma^{ind}_{particle} + \gamma^{ind}_{EDL}\right) a^2 \left(\lambda^0\right)^2}{12\pi^2 \varepsilon_m \varepsilon_0 \mu r_0^3} \tag{19}$$

The total polarizability of the screened particle $\gamma^{ind}_{screened}$ as well as polarizabilities of the particle $\gamma^{ind}_{particle}$ and EDL associated with it γ^{ind}_{EDL} are functions of the ratio of the radius of the particle, a, to the Debye length $1/k$, that is ka, particle zeta potential, ζ, and the $\varepsilon_p/\varepsilon_m$ ratio and temperature of the medium. For the typical case of aqueous suspension of dielectric particles (e.g., virus, bacteria, and latex beads) at 25°C, when $\varepsilon_p \sim 2$, $\varepsilon_m \sim 80$, $|\zeta| = 50$ mV [48] (we use here the absolute value of zeta potential $|\zeta|$ in accordance with Equation (5.74) in Ref. [48]) calculated value of $\gamma^{ind}_{screened} \sim 6$ for $ka \sim 1$ (see Figure 5.7a in Ref. [48]) and $\gamma^{ind}_{screened} \sim 0.5$ for $ka \sim 5$. These total induced polarizabilities of the screened particles $\gamma^{ind}_{screened}$ allow the explanation of the high removal efficiency for MS2 bacteriophage at pH 3 (Tables 2 and 3) as well as good *fr* bacteriophage removal efficiencies at pH in the range from 5 to 9 (see Tables 6 and 7 later) that are below their PZC values of 3.9 and ~8.9–9.0, respectively.

Assuming that λ is equal to the calculated value of λ° =2.8 μC/m (Equation (5)), the estimated strength of electric field in the *near field* zone (at ionic strength of 0.1 mM up to 32 nm from the surface of alumina nanofiber, that is, at $r_0 \sim 0.6$ μm) is $E_y \sim 10^7$ V/cm. This value is 1–2 orders of magnitude greater than the typical values for the screened Stern layer that is assumed to be on the order of ion size [49].

3.4. *Electrokinetic motion of MS2 and* E. coli *in electric field of assembly*

Table 4 shows dependence of MS2 and *E. coli* removal efficiencies by the assemblies at 0.15- and 0.012-g/L loadings vs. contact time. No centrifugation step was performed in this case. Results indicate that MS2 and *E. coli* particles have similar average velocities at two different loadings of 0.15 and 0.012 g/L in the electric field created by the assemblies. Moreover, the calculated and experimental values of average velocities for MS2 bacteriophage are similar as well.

Table 4. Dependence of MS2 and *E. coli* removal by assembly vs. contact time at pH 7.

MS2 or *E. coli*	Solid load (g/L)	R_m (Ω·m)[a]	$1/k$ (nm)[b]	ka[b]	γ[c]	$v^{calc.}$ (μm/s)[d]	Contact time, $t_{cont.}$ (s)	MS2 or *E. coli* removal (LRV)	r_0 (μm)[e]	v^{exp} (μm/s)[f]
MS2	0.15	47	8.9	1.5	2	53	2	4.5 ± 0.2	86	43
							8	4.7 ± 0.3	86	
							30	5.2 ± 0.1	87	
	0.012	147	32	0.4	5	149	2	0.4 ± 0.2	83	42
							8	0.5 ± 0.1	100	
							30	0.6 ± 0.2	116	
							120	0.9 ± 0.7	156	
E. coli	0.15	32					2	0.8 ± 0.4	41	21
							8	2.2 ± 0.7	72	
							30	2.6 ± 0.8	76	
	0.012	99					2	0.24 ± 0.13	53	27
							8	0.9 ± 0.8	156	
							30	1.2 ± 0.5	188	

Notes: [a]Resistivity of the dispersive medium; [b]Debye length (see footnote 'a' in Table 1); [c]$\gamma^{ind}_{screened} = \gamma^{ind}_{particle} + \gamma^{ind}_{EDL}$; [d]Equation (19); [e]distance that MS2 or *E. coli* travels from the farthest point P in the plane of the assembly with $x = 0$ at the center and $y = r_0$ to the surface of the assembly during a certain time interval; [f]$v^{exp} = r_0/t_{cont.}$

3.5. *Electrophoretic mobility of MS2*

The electrophoretic mobility, μ, is defined as a ratio of field-induced particle velocity, v, to the homogeneous field strength, E_{ext}, in the liquid at a large distance from the particles. In the present case, we can define an average static electrophoretic mobility $\langle\mu\rangle$ as:

$$\langle\mu\rangle = \frac{\langle v\rangle}{\langle E\rangle} \tag{20}$$

It should be noted that dielectrophoretic velocity $v^{de}_{screened}$ is a quadratic function of the strength of electric field (Equation (18)).

From the data given in Table 4 for flow velocity and the electrophoretic mobility in aqueous solution of $\mu \approx 3$ μm/s/V/cm at ionic strength of 3 mM (approximately −2.5 log [Na^+]) [50], we can estimate average strength of the electric field $\langle E\rangle$ in the solution as ~14 V/cm at $r_0/2 = 43$ μm (Table 4). This value is in a good agreement with the electrophoretic velocity calculated with the use of Helmholtz–Smoluchowski equation for electrophoresis [51]:

$$v_e = \frac{\varepsilon_m \varepsilon_0 \zeta}{\mu} E \tag{21}$$

where ζ is the zeta potential. The average strength of electric field in aqueous solution at 25°C with v_e of 86 μm/s (Table 4) and ζ(MS2) = −40.4 ± 3.7 mV [39] at pH 7 can be estimated at 15.2 V/cm. This good agreement in the electrophoretic velocities obtained from data for electrophoretic mobility [50] and from Helmholtz–Smoluchowski equation for electrophoresis [51] indicates that the characteristic time scale for attracting and

adsorbing of MS2 and *E. coli* particles in aqueous suspensions of the assemblies at 0.15- and 0.012-g/L loadings is about 2 s, which is consistent with formation times of haloes (2–4 s) by the Indian ink particles [14].

3.6. *Viruses, bacteriophages, and bacteria adsorption by alumina nanofiber nonwoven media*

Table 5 shows virus, bacteriophage, and bacteria removal efficiencies by a single layer of alumina nanofiber media by either a pleated cartridge or a 25-mm-diameter disk at flow velocity in the range from 0.7 to 1.4 mm/s. Initial removal efficiencies by 0.8-mm-thick media reported in Table 6 are high for viruses, bacteriophages, and bacteria. Most bacteria and most other contaminants encountered in nature are electronegatively charged in water [52]. A notable exception is *fr* bacteriophage that is electropositive at pH less than about 8.9–9.0 [41]. Yet, the initial removal efficiency for the *fr* at pH 7 is high as well, i.e.,

Table 5. Bacteriophage, bacteria, and virus removal efficiencies by alumina nanofiber media at pH 7.

Organism	Species	Size (μm)	Initial removal efficiency (%)
Virus	Poliovirus 1	0.025–0.030	>99.92 ± 0.01[a,b]
	Echovirus 1	0.050–0.080	>99.98 ± 0.00[a,b]
	Coxsackievirus B5	0.027	>99.991 ± 0.01[a,b]
	Adenovirus	0.070–0.090	>99.997 ± 0.00[a,b]
Bacteriophage	MS2	0.027	>99.9999[c,d]
	fr	0.020	>99.9999[c,d]
Bacteria	*E. coli*	0.5[e]–2[f]	>99.99999[c,d]
	Raoultella terrigena	(0.3–1)[e]·(0.6–6)[f]	>99.99999[c,g]
	Acholeplasma laidlawii	(<0.2)[e]·(~0.5)[f]	99.95 ± 0.05[c,d]

Note: [a]Ref. [53 © [American Society for Microbiology]. Reproduced by permission of American Society for Microbiology.]; [b]with the use of VS2.5-5 cartridge (available from Argonide Corporation); [c]present work; [d]25-mm-diameter, 0.8-mm-thick filter disk (available from Argonide Corporation); [e]diameter; [f]length.

Table 6. Bacteriophage *fr* adsorption by alumina nanofiber assembly at pH 7.

Solid load (g/L)	pH	Conductivity (mS/cm)	$1/k$ (nm)[a]	Average distance between two assemblies, $2A$ (μm)[b]	*fr* removal efficiency (LRV)	r_0 (Equation (15)) (μm)[c]	ka[d]
3	10	4.0	2.0	40	−0.12 ± 0.12	0.0 ± 1.5	4.8
	9	3.5	2.0	40	2.0 ± 0.2	15.7 ± 0.7	4.8
	7	3.5	2.0	40	4.2 ± 0.3	19.2 ± 0.2	4.8
	5	3.6	2.0	40	4.1 ± 0.3	19.1 ± 0.2	4.8
0.15	9	0.34	8.9	177	0.14 ± 0.10	9 ± 6	1.1
	7	0.32	8.9	177	0.26 ± 0.16	16 ± 9	1.1
	6	0.32	8.9	177	0.27 ± 0.06	17 ± 4	1.1
	5	0.33	8.9	177	0.39 ± 0.03	23 ± 2	1.1

Note: [a]Debye length (see footnote 'a' in Table 1); [b]Equation (7); [c]distance that *fr* travels from the farthest point P in the plane of the assembly with $x = 0$ at the center and $y = r_0$ to the surface of the assembly in 8 min; [d]a is the radius of *fr*.

Table 7. *fr* bacteriophage removal efficiencies by alumina nanofiber media as a function of pH.

		Initial removal efficiency (%)		
pH	Conductivity (μS/cm)	One layer	Two layers	ζ potential (mV)
3	495	99.9 ± 0.2	99.999 ± 0.003	−4[a]
5	41	>99.99994	>99.99994	16 ± 2[a]
7	34	>99.99994	>99.99994	47 ± 9[a]
8	74	>99.99992	>99.99992	46 ± 6[a]
9	70	>99.9999	>99.9999	26 ± 4[a]
10	80	99.994 ± 0.004	>99.9999	23[a]
11	1180	37 ± 16	97 ± 45	~0[a]

Note: [a]present work.

>99.9999% [54] with a single layer of the media at a flow velocity 0.7 mm/s. Results of Tables 6 and 7 show good adsorption of *fr* bacteriophage in electric field of assembly dispersed in aqueous solution.

3.7. Latex beads adsorption by alumina nanofiber assembly

Figure 4(a) shows SEM images of 30-nm latex beads partially covering alumina nanofiber media. In this case, a single drop of latex beads dispersion was deposited onto a dry media. Figure 4(b) shows significant change in latex beads morphology while the suspension of latex beads was either filtered through the wet media or adsorbed by the assemblies in the mulch. This remarkable change in morphology is a consequence of polarization effect induced by the external field created by the assembly in aqueous solution (see Equation (15)). In the former case, it appears that there was not enough time for the beads to acquire additional charge via the polarization effect because the media were originally dry and there was not enough torque to rotate the bead (see Equation (17)). This change in latex beads morphology was further studied by secondary ion mass spectrometry run in the event-by-event bombardment/detection mode [55,56].

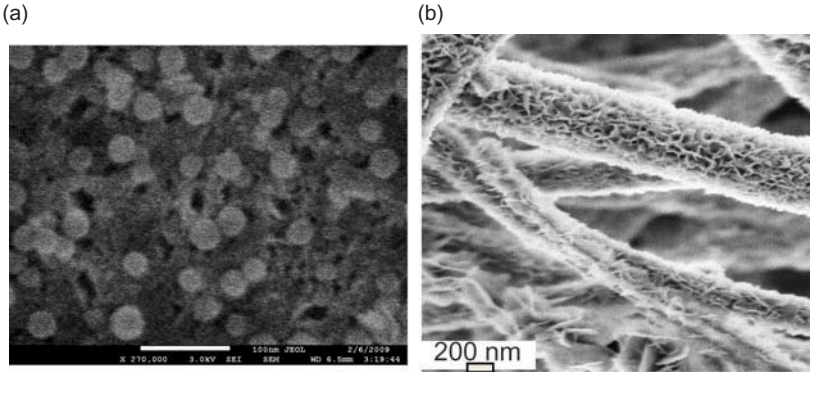

Figure 4. (a) SEM image of 30-nm latex beads partially covering assembly; (b) SEM image of 30-nm latex beads that changed morphology from spherical to flake-like.

It should be noted that no such a polarization effect was evident while filtering *E. coli* bacteria by alumina nanofiber media from dry airstream. However, the same media remove *E. coli* bacteria from an airstream with 99.9992% efficiency [31] at relative humidity close to 100% due to the polarization effect induced by the *E. coli* bacteria in the wet media.

If one assumes that negatively charged surface of a 30-nm latex bead is exposed to N_{AlOOH}, the number of nanoalumina fibers than the total positive electric charge 'seen' by the latex bead (see Equation (3)) is:

$$Q_{AlOOH} \sim 780 \cdot e \cdot N_{AlOOH} \tag{22}$$

From Figure 2, we can assume that N_{AlOOH} is approximately equal to 20, and nanoalumina fibers are evenly distributed on the surface of a half sphere around a latex sphere with radius $R = l_{AlOOH}$ and $Q_{bead} \sim 100 \cdot e$, then the force acting on the bottom of the 30-nm bead can be estimated as:

$$F_z = E_z Q_{bead} = \frac{\sigma^0_{AlOOH} Q_{bead}}{4\varepsilon_0 \varepsilon_m} \approx 4.6 \times 10^{-10} N \tag{23}$$

where a thin half sphere, uniformly charged with charge density σ^0, creates the electric field at the center of the sphere of $\sigma^0/4\pi\varepsilon_0\varepsilon_m$ with the z-component coinciding with the symmetry axis of the half sphere. Differential pressure acting on the negatively charged bottom part of a soft latex bead is:

$$\Delta P = \frac{F_z}{S_{bead}/2} = \frac{2F_z}{\pi D^2_{bead}} = 320,000 \text{ Pa} \sim 3.2 \text{ bar} \tag{24}$$

This differential pressure acting on the negatively charged bottom part of a soft latex bead appears to be enough to transform spherical particle into a flake. No organic solvents were used during the remarkable change in the morphology of latex particles seen in Figure 4. It should be noted that alumina nanofiber media adsorb 30-nm-diameter latex beads with even greater efficiency from methyl and ethyl alcohols and their mixtures. For example, the capacity of 25-mm-disk for removal of 30-nm-diameter latex beads at an input concentration of 10^{13} particles/mL is 1.45×10^{14} beads [57] in water suspension. This compares to 1.0×10^{15} beads in ethyl alcohol and greater than 1.5×10^{15} beads in a 50%/50% mixture of methyl/ethyl alcohol.

4. Conclusions

This article demonstrates how strong electropositive charge properties of alumina nanofiber assemblies dispersed in polar liquids and nonwoven media can be used as a means of collecting and separating submicron and micron particles such as viruses, bacteriophages, bacteria, and latex spheres. The assembly creates a strong electric field that extends as far as 0.3 mm from alumina nanofiber surface into an aqueous dispersive medium. This is many orders of magnitude (>4) greater than that predicted by the DLVO theory.

The nonwoven media adsorb submicron particles predominately on the basis of a combination of their inherent charge and acquired induced polarization charge, rather than by physical entrapment based on particle size. The media have a high dynamic response for adsorption, allowing purification within a very shallow bed and at flow rates at an

order of magnitude greater than that can be achieved with an ultraporous membrane. A given particle can be eluted by replacement with one that is more adherent. For instance, viruses can be lifted off the media by replacement with beef extract. The media are suggested for purification of virus and proteins, where a high dynamic binding capacity is combined with high flow velocities at low differential pressure. Chromatographic separations of a range of submicron particles of biological relevance such as viruses, chromosomes, DNA, RNA, and macromolecules at pressure drops less than 1 bar over ambient, in thin beds with high flow rates appear feasible.

Strong electron field emission from the alumina nanofiber/microglass assembly was measured, and we *speculate* that it might be similar to that of electron field emission from carbon nanotubes [58]. It is a quantum effect where under a sufficiently high external electric field, electrons near the Fermi level can tunnel through the energy barrier and escape to the vacuum level.

After more than a century of the research in the field of colloid science pioneered by Helmholtz in 1853, interactions between charged colloidal particles are still a very puzzling matter. A high-level quantum mechanical research is needed to resolve the controversy between the DLVO and the Sogami theories. Whatever the mechanism of attraction and adsorption of nanosize and micron-size particles by alumina nanofiber assembly presented in this work, the long-range phenomena are novel and striking and may have important implications not only for surface science but also for physics and life sciences.

Acknowledgments

We thank Mr R. Ristau of IMS, University of Connecticut, for providing us with TEM and SEM images of alumina nanofibers bonded to glass and lyocell microfibers (Figures 1 and 2) and Dr S. V. Verkhoturov of Texas A&M University for providing us with SEM images of latex beads covering alumina nanofiber assemblies (Figure 4) and for providing us with preliminary data on strong electron field emission from the alumina nanofiber/microglass assembly.

References

[1] G. Gouy, *Sur la constitution de la charge electrique a la surface d'un electrolyte*, Compt. Rend. 149 (1910), pp. 654–657.
[2] D.L. Chapman, *LI.A contribution to the theory of electrocapillarity*, Philos. Mag. 25 (1913), pp. 475–481. doi:10.1080/14786440408634187.
[3] O. Stern, *The theory of electrolytic double layer*, Z. Electrochem. 30 (1924), pp. 508–516.
[4] A.V. Delgado, F. González-Caballero, R.J. Hunter, L.K. Koopal, and J. Lyklema, *Measurement and interpretation of electrokinetic phenomena (IUPAC technical report)*, Pure Appl. Chem. 77 (2005), pp. 1753–1805. doi:10.1351/pac200577101753.
[5] H. Zhang, A.A. Hassanali, Y.K. Shin, C. Knight, and S.J. Singer, *The water-amorphous silica interface: Analysis of the stern layer and surface conduction*, J. Chem. Phys. 134 (2011), p. 024705. doi:10.1063/1.3510536.
[6] D.J. Bonthuis and R.R. Netz, *Unraveling the combined effects of dielectric and viscosity profiles on surface capacitance, electro-osmotic mobility, and electric surface conductivity*, Langmuir. 28 (2012), pp. 16049–16059. doi:10.1021/la3020089.
[7] T.F. Tadros and J. Lyklema, *Adsorption of potential-determining ions at the silica-aqueous electrolyte interface and the role of some cations*, J. Electroanal. Chem. & Interfacial Electrochem. 17 (1968), pp. 267–275. doi:10.1016/S0022-0728(68)80206-2.
[8] A.S. Dukhin and P.J. Goetz, *Characterization of Liquids, Nano- and Microparticulates, and Porous Bodies Using Ultrasound*, 2nd ed., Elsevier, Amsterdam, 2010.

[9] B.V. Derjaguin and L. Landau, *Theory of stability of strongly charged lyophobic sols of the adhesion of strongly charge particles in solution electrolytes (in russian)*, Acta Physicochim. USSR. 14 (1941), pp. 633–662.
[10] E.J. Verwey and J.T.G. Overbeek, *Theory of the Stability of Lyophobic Colloids*, Elsevier, Amsterdam, 1948.
[11] J. Israelachvili, *Intermolecular and Surface Forces*, Academic Press, San Diego, CA, 1992.
[12] T. Tadros, *General principles of colloid stability and the role of surface forces,* in *Colloid Stability: The Role of Surface Forces*, Part I, T.F. Tadros, ed., Willey-VCH, Weinheim, 2006, pp. 1–22. doi:10.1002/9783527631070.ch1
[13] F. Borghi, V. Vyas, A. Podestà, P. Milani, and R.G. Haverkamp, *Nanoscale roughness and morphology affect the isoelectric point of titania surfaces*, Plos ONE. 8 (2013), p. e68655. doi:10.1371/journal.pone.0068655.
[14] B.V. Derjaguin and M.V. Golovanov, *On long-range forces of repulsion between biological cells*, Colloids and Surfaces. 10 (1984), pp. 77–84. doi:10.1016/0166-6622(84)80009-8.
[15] H. Rivera, J.K. Pollock, and H.A. Pohl, *The ac field patterns about living cells*, Cell Biophys. 7 (1985), pp. 43–55. doi:10.1007/BF02788638.
[16] H.A. Pohl, *Dielectrophoresis*, Cambridge University Press, Cambridge, UK, 1978.
[17] A.S. Dukhin, Z.R. Ulberg, V.I. Karamushka, and T.G. Gruzina, *Peculiarities of live cells' interaction with micro- and nanoparticles*, Adv. Colloid & Interface Sci. 159 (2010), pp. 60–71. doi:10.1016/j.cis.2010.05.004.
[18] V.A. Murtsovkin, *Nonlinear flows near polarized disperse particles*, Colloid J. 58 (1996), pp. 341–349.
[19] M.Z. Bazant and T.M. Squires, *Induced-charge electrokinetic phenomena*, Curr. Opin. Colloid Interface Sci. 15 (2010), pp. 203–213. doi:10.1016/j.cocis.2010.01.003.
[20] I. Sogami, *Effective potential between charged spherical particles in dilute suspension*, Phys. Lett. 96 (1983), pp. 199–203. doi:10.1016/0375-9601(83)90704-1.
[21] I. Sogami and N. Ise, *On the electrostatic interaction in macroionic solutions*, J. Chem. Phys. 81 (1984), pp. 6320–6332. doi:10.1063/1.447541.
[22] N. Ise and H. Yoshida, *Paradoxes of the repulsion-only assumption*, Acc. Chem. Res. 29 (1996), pp. 3–5. doi:10.1021/ar950019k.
[23] B.V.R. Tata, E. Yamahara, P.V. Rajamani, and N. Ise, *Amorphous clustering in highly charged dilute poly(chlorostyrene-styrene sulfonate) colloids*, Phys. Rev. Lett. 78 (1997), pp. 2660–2663. doi:10.1103/PhysRevLett.78.2660.
[24] N. Ise, *Recent study on counterion-mediated attraction between colloidal particles*, Colloids Surfaces. 146 (1999), pp. 347–357. doi:10.1016/S0927-7757(98)00775-4.
[25] N. Ise, *Ordering of ionic solutes in dilute solutions through attraction of similarly charged solutes – A change of paradigm in colloid and polymer chemistry*, Angew. Chem. Int. Ed. Engl. 25 (1986), pp. 323–334. doi:10.1002/anie.198603231.
[26] J.-M. Zheng and G.H. Pollack, *Long-range forces extending from polymer-gel surfaces*, Phys. Rev. E. 68 (2003), p. 031408. doi:10.1103/PhysRevE.68.031408.
[27] J.-M. Zheng and G.H. Pollack, *Solute exclusion and potential distribution near hydrophilic surfaces*, in *Water and the Cell*, G.H. Pollack, I.L. Cameron, and D.N. Wheatley, eds., Springer, Dordrecht, 2006, pp. 165–174.
[28] I. Sogami, *Long-range attractive tail of colloidal interaction*, Chem. Lett. 41 (2012), pp. 1331–1333. doi:10.1246/cl.2012.1331.
[29] F. Tepper and L. Kaledin, *Nanosize electropositive fibrous adsorbent*. US patent application 20030127393, 2003.
[30] F. Tepper and L. Kaledin, *Nanostructured chem-bio non-woven filter*, in *Nanoscience and Nanotechnology for Chemical and Biological Defense*. *ACS Symposium Series*, Vol. 1016, Chapter 21, R. Nagarajan, W. Zukas, T.A. Hatton, and S. Lee, eds., American Chemical Society, Washington, DC, 2009, pp. 273–288.
[31] R. Al-Shakhshir, F. Regnier, J.L. White, and S.L. Hem, *Effect of protein adsorption on the surface charge characteristics of aluminium-containing adjuvants*, Vaccine. 12 (1994), pp. 472–474. doi:10.1016/0264-410X(94)90127-9.
[32] D.R.U. Knappe, K. Li, P.A. Quinlivan, and T.B. Wagner, *Effects of Activated Carbon Characteristics on Organic Contaminant Removal*, IWA Publishing, Denver, CO, 2003.
[33] G.M. Tom and L.J. Haltquist, *Channelized sorbent media, and methods of making same*, US patent 6764755, 2004.

[34] W.H. Gitzen, *Alumina as a Ceramic Material*, American Ceramic Society, Special Publication 4, Westerville, 1970.
[35] L. Ermakova, N. Bogdanova, M. Sidorova, and J. Lyklema, *Electrosurface characteristics of oxide nanolayers and nanopore membrane in electrolyte solutions*, in *Nanoscience. Colloidal and Interfacial Aspects*, Surfactant Science Series 147, V.M. Starov, ed., CRS Press, Boca Raton, FL, 2010, pp. 193–220.
[36] K. Leschonski, *Representation and evaluation of particle size analysis data*, Part. Charact. 1 (1984), pp. 89–95. doi:10.1002/ppsc.19840010115.
[37] O.D. Velev, K. Furusawa, and K. Nagayama, *Assembly of latex particles by using emulsion droplets as templates. 1. Microstructured hollow spheres*, Langmuir. 12 (1996), pp. 2374–2384. doi:10.1021/la9506786.
[38] B. Michen and T. Graule, *Isoelectric points of viruses*, J. Appl. Microbiology. 109 (2010), pp. 388–397.
[39] A. Duek, E. Arkhangelsky, R. Krush, A. Brenner, and V. Gitis, *New and conventional pore size tests in virus-removing membranes*, Water Res. 46 (2012), pp. 2505–2514. doi:10.1016/j.watres.2011.12.058.
[40] C.V. Chrysikopoulos and V.I. Syngouna, *Attachment of bacteriophages MS2 and ΦX174 onto kaolinite and montmorillonite: Extended-DLVO interactions*, Colloids and Surfaces B: Biointerfaces. 92 (2012), pp. 74–83. doi:10.1016/j.colsurfb.2011.11.028.
[41] G. Herath, K. Yamamoto, and T. Urase, *Removal of viruses by microfiltration membranes at different solution environments*, Water Sci. Technol. 40 (1999), pp. 331–338. doi:10.1016/S0273-1223(99)00515-6.
[42] D.-Q. Lin, P.J. Brixius, J.J. Hubbuch, J. Thömmes, and M.-R. Kula, *Biomass/adsorbent electrostatic interactions in expanded bed adsorption: A zeta potential study*, Biotechnol. Bioeng. 83 (2003), pp. 149–157. doi:10.1002/bit.10654.
[43] I.L. Pepper and C.P. Gerba, *Environmental Microbiology. A Laboratory Manual*, 2nd ed., Elsevier AP, Amsterdam, 2004.
[44] Microbiological Water Purifiers, *NSF Protocol P231*, NSF International, Ann Arbor, MI, 2008.
[45] L. Kaledin, F. Tepper, O. Vargas, and T. Kaledin, *Solid Phase Extraction of Nanosize Particles by Nanoalumina Depth Media*. ENT magazine, March–April 2010, pp. 78–85.
[46] J. Lyklema, *Fundamentals of Interface and Colloid Science: Solid-Liquid Interfaces* Vol. 2, Chapter 3, Academic Press, London, 1995.
[47] A.L. Stanford and J.M. Tanner, *Physics for Students of Science and Engineering*, HBJ Publishers, San Diego, CA, 1985.
[48] V.N. Shilov and O.A. Shramko, *Nonlinear electrokinetic phenomena in nanosized dispersions*, in *Nanoscience. Colloidal and Interfacial Aspects Surfactant Science Series, 147*, V.M. Starov, ed., CRS Press, Boca Raton, FL, 2010, pp. 101–127.
[49] N.I. Lebovka and O.L. Alexeev, *Electroosmosic flow in micro- and nanosized systems*, in *Nanoscience Colloidal and Interfacial Aspects*, *Surfactant Science Series 147*, V.M. Starov, ed., CRS Press, Boca Raton, FL, 2010, pp. 129–164.
[50] S.E. Mylon, C.I. Rinciog, N. Schmidt, L. Gutierrez, G.C.L. Wong, and T.H. Nguyen, *Influence of salts and natural organic matter on the stability of bacteriophage MS2*, Langmuir. 26 (2010), pp. 1035–1042. doi:10.1021/la902290t.
[51] M. Smoluchowski, *Zur theorie der elektrischen kataphorese und der ober-henleitung*, Phys. Z. 6 (1905), pp. 529–531.
[52] E.A. Ostreicher, T.E. Arnold, and R.S. Conway. *Charge modified filter media,* in *Filtration and Purification in the Biopharmaceutical Industry*, 2nd ed., Vol. 174, M.W. Jornitz and T.H. Meltzer, eds., Informa Healthcare, New York, 2008, pp. 23–46.
[53] L.A. Ikner, M. Soto-Beltran, and K.R. Bright, *New method using a positively charged microporous filter and ultrafiltration for concentration of viruses from tap water*, Appl. Environ. Microbiol. 77 (2011), pp. 3500–3506. doi:10.1128/AEM.02705-10
[54] F. Tepper, L. Kaledin, O. Vargas, and T. Kaledin, *Wide particle size spectrum, high efficiency pleated filter*, International Water Conference, IWC-10-47, October 24–28, San Antonio, TX, 2010.
[55] V.T. Pinnick, S.V. Verkhoturov, L. Kaledin, Y. Bisrat, and E.A. Schweikert, *Molecular identification of individual nano-objects*, Anal. Chem. 81 (2009), pp. 7527–7531. doi:10.1021/ac9014337.

[56] V. Pinnick, S. Rajagopalachary, S.V. Verkhoturov, L. Kaledin, and E.A. Schweikert, *Characterization of individual nano-objects by secondary ion mass spectrometry*, Anal. Chem. 80 (2008), pp. 9052–9057. doi:10.1021/ac8014615.

[57] F. Tepper, L. Kaledin, and T. Kaledin, *Non-woven electrostatic media for chromatographic separation of biological particles*, J. Liq. Chromatogr. Relat. Technol. 32 (2009), pp. 607–627. doi:10.1080/10826070802711006.

[58] Y. Cheng and O. Zhou, *Electron field emission from carbon nanotubes*, C. R. Physique. 4 (2003), pp. 1021–1033. doi:10.1016/S1631-0705(03)00103-8.